

Systematic partitioning of proteins for quantum-chemical fragmentation methods using graph algorithms

Mario Wolter,[†] Moritz von Looz,^{‡,¶} Henning Meyerhenke,^{*,‡} and
Christoph R. Jacob^{*,†}

[†]*Institute of Physical and Theoretical Chemistry, Technische Universität Braunschweig,
Gaußstr. 17, 38106 Braunschweig, Germany*

[‡]*Department of Computer Science, Humboldt-Universität zu Berlin, Unter den Linden 6,
10099 Berlin, Germany*

[¶]*Now at Advanced Concepts Team, European Space Research and Technology Center,
Noordwijk, The Netherlands*

E-mail: meyerhenke@hu-berlin.de; c.jacob@tu-braunschweig.de

Abstract

Quantum-chemical fragmentation methods offer an efficient approach for the treatment of large proteins, in particular if local target quantities such as protein–ligand interaction energies, enzymatic reaction energies, or spectroscopic properties of embedded chromophores are sought. However, the accuracy that is achievable for such local target quantities intricately depends on how the protein is partitioned into smaller fragments. While the commonly employed naïve approach of using fragments with a fixed size is widely used, it can result in large and unpredictable errors when varying the fragment size. Here, we present a systematic partitioning scheme that aims at minimizing the fragmentation error for a given maximum fragment size. To this end, we construct a weighted graph representation of the protein, in which the amino acids constitute the nodes. These nodes are connected by edges weighted with an estimate for the fragmentation error that is expected when cutting this edge. This allows us to employ graph partitioning algorithms provided by computer science to determine near-optimal partitions of the protein. We apply this scheme to a test set of six proteins representing various prototypical applications of quantum-chemical fragmentation methods and show that our graph-based scheme consistently improves upon the naïve approach.

1 Introduction

Computer simulations have become an essential tool for investigating the chemical and physical mechanisms underlying the functionality of biomolecules.^{1,2} With the development of classical force fields and increasingly powerful computational resources, structural investigation of biomolecules, comprised of up to hundred thousands of atoms, have become possible.^{3,4} However, in many cases quantum-chemical methods are essential for accurately modeling biomolecular systems. Examples include the accurate prediction of protein–ligand interaction energies,⁵ the calculation of spectroscopic properties of chromophores embedded in proteins,^{6–8} and the modeling of enzymatic reactions.^{9,10}

In the past decades, enormous progress has been made to increase the computational efficiency of quantum-chemical methods for large molecular systems. Efficient implementations nowadays allow for a full treatment of biomolecules containing up to thousands of atoms.^{11–13} A particularly appealing strategy for the quantum-chemical treatment of large biomolecular systems is provided by fragmentation methods (for reviews, see, e.g., Refs. 14–16). Such methods partition a biomolecule into many smaller, possibly overlapping fragments, which are each treated individually. This generally leads to a natural linear scaling of the computational effort with the number of fragments, and thus significantly reduces the computational effort required for a treatment of the full biomolecular system. Moreover, the many independent calculations for the different fragments can easily be performed in an embarrassingly parallel fashion.

Numerous flavors of such fragmentation methods that are applicable to biomolecules have been developed. The original molecular fractionation with conjugate caps (MFCC) approach^{17–19} partitions a protein into single amino acid residues, which are saturated with suitable capping groups, and performs separate quantum-chemical calculations for each resulting fragment. Such a treatment can be combined with the use of an embedding potential in the fragment calculations.^{20,21} For instance, the MFCC method can be combined with an electrostatic embedding potential.^{22,23} The fragment molecular orbital (FMO) method^{24–28}

employs a more sophisticated embedding potential in combination with a frozen-orbital treatment of the fragment boundaries. One of us has previously developed an extension of the frozen-density embedding (FDE) scheme^{29,30} for the subsystem treatment of proteins, which employs the MFCC partitioning in combination with a density-based embedding potential (termed 3-FDE).³¹

Fragmentation methods can be particularly useful if one is interested in properties that are local to a specific part of a biomolecular system. In this case, they make it possible to selectively tune the accuracy of the local target quantities by employing a more accurate quantum-chemical description for fragments that are closer to the relevant region, while a less accurate description can be used for distant fragments. Such a strategy can, for instance, be employed in the calculation of protein–ligand interaction energies, which demand an accurate description of the protein’s binding pocket, while for other parts of the protein the accuracy is less crucial.^{32,33} Another example is the calculation of spectroscopic properties of chromophores embedded in proteins. Here, fragmentation methods can be used to obtain an electron density of the protein, which can be included in the calculation of the chromophores’ spectroscopic properties, e.g., via a frozen-density embedding potential.^{34,35} Again, in such a setup more accurate quantum-chemical methods could be used for fragments that are closer to the chromophores. We note that, in contrast to QM/MM methods,^{36,37} fragmentation methods generally maintain a quantum-chemical description for the whole protein.

A central issue in all fragmentation methods is the suitable choice of the fragments, i.e., the partitioning scheme used for decomposing the large biomolecular system into smaller subsystems. This choice requires a trade-off between efficiency and accuracy: In general, using a smaller number of larger fragments will reduce the overall computational effort, but will at the same time increase the error caused by the fragmentation. In the simplest and most common partitioning scheme, fragments consisting of a fixed number of amino acids along the backbone chain are used.³² Antony and Grimme assessed such an approach for the calculation of protein–ligand interaction energies with MFCC and found a rather

irregular dependence of the fragmentation error on the fragment size instead of a smooth convergence.³⁸ Thus, particularly for localized target quantities, the resulting fragmentation error can be highly dependent on the precise choice of the fragments.

A number of partitioning schemes aim to address this issue with a more sophisticated definition of the relevant fragments. In the generalized MFCC scheme, overlapping fragments are defined based on chemical connectivity and spatial proximity such that relevant chemical interactions (e.g., hydrogen bonds between different chains) are included within the fragments.^{22,39} Similarly, the generalized energy-based fragmentation approach uses a distance cut-off when partitioning a protein into fragments.^{40,41} The molecular tailoring approach (MTA) combines such a distance criterion with an algorithm for the iterative combination of fragments, which also accounts for chemical connectivity information.^{42–44} However, all these schemes aim at the overall error in global properties of the full protein instead of the error in local target quantities such as protein–ligand interaction energies or spectroscopic properties.

Here, we present a systematic partitioning scheme that is tailored to the calculation of local target quantities, such as protein–ligand interaction energies or local spectroscopic properties, with quantum-chemical fragmentation methods. Our partitioning scheme is constructed such that the expected fragmentation error in the target quantity is minimized, subject to constraints on the fragment size and/or the number of fragments. To this end, we map the biomolecular system to a graph representation, in which the nodes represent amino acid residues and the edges describe interactions between them. Each edge is weighted with an estimate of the error in the target quantity that is expected when cutting this edge, i.e., when assigning the nodes connected by this edge to different fragments.

Using this representation, graph partitioning algorithms⁴⁵ can be used to find a fragmentation that minimizes the *edge cut weight*, (i.e., the sum of the weights of the edges between different fragments), which corresponds to the expected error in the local target quantity. We have previously put forward this idea and have presented suitable graph parti-

tioning algorithms that include additional chemical constraints on the resulting partition.⁴⁶ However, as the focus of this earlier work was on the algorithm engineering aspects, it did not include any quantum-chemical calculations and only considered graphs that were constructed in an *ad hoc* fashion. Here, we close this gap by applying our earlier ideas to actual quantum-chemical fragmentation calculations. We address the construction of suitable graph representations and carefully assess the accuracy of local target quantities with the resulting fragmentations. We show that our graph-based, systematic partitioning scheme significantly improves the accuracy compared to the commonly used, simpler alternative schemes, while not increasing the overall computational effort.

This work is organized as follows. In Sect. 2 we review the quantum-chemical fragmentation strategy employed here (Sect. 2.1), introduce measures for quantifying the fragmentation error (Sect. 2.2), and present the methodology for mapping the fragmentation of proteins to a graph partitioning problem (Sects. 2.3, 2.4, and 2.5). The computational details are given in Sect. 2.6. This is followed by a first test and assessment of our methodology for ubiquitin in Sect. 3. Finally, a larger test set of five additional proteins is considered in Sect. 4. Conclusions are drawn and an outlook is given in Sect. 5.

2 Methodology

2.1 Fragmentation methods for proteins

All quantum-chemical fragmentation methods have in common that they partition a large biomolecular system into smaller subsystems. When considering the electron density, they commonly approximate the total system’s electron density $\rho_{\text{tot}}(\mathbf{r})$ as

$$\rho_{\text{tot}}(\mathbf{r}) \approx \rho_{\text{tot}}^{\text{fragm}}(\mathbf{r}) = \sum_i \rho_i(\mathbf{r}) - \sum_j \rho_j^{\text{cap}}(\mathbf{r}), \quad (1)$$

where $\rho_i(\mathbf{r})$ is the electron density of the i -th fragment, in which dangling bonds have been saturated with suitable capping groups, and $\rho_j^{\text{cap}}(\mathbf{r})$ are the densities of capping molecules that serve to correct for these capping groups. This fragmentation can be formulated in a more general way using the inclusion–exclusion principle.⁴⁷

The MFCC method^{17–19} uses the above fragmentation of the electron density, and employs amino acids (or groups of amino acids) as fragments. These are cut at the peptide bonds, and $-\text{CO}-\text{CH}_3$ and $-\text{NH}-\text{CH}_3$ capping groups are introduced to preserve the polarity of the peptide bond. For each cut peptide bond, these capping groups are then joined to an N-methyl-acetamide molecule, which is subtracted to correct for the introduced capping groups. In the original MFCC method, quantum-chemical calculations are performed for the isolated fragments as well as cap molecules. Numerous other fragmentation methods are derived from the MFCC scheme.^{14,15}

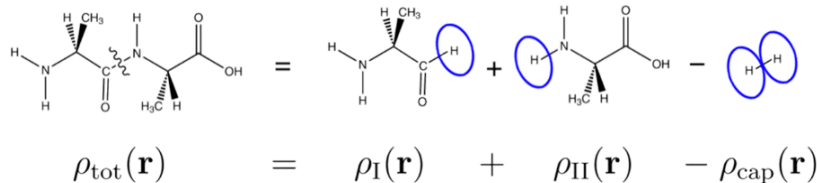


Figure 1: Illustration of the fragmentation used in the simplified MFCC scheme with hydrogen caps that is employed throughout this work.

Here, we aim to develop a partitioning scheme that is independent of the specific fragmentation method that is used. Therefore, in this work we consider only a simplified MFCC scheme in which hydrogen atoms are used as capping groups. The fragmentation and capping strategy used in this simplified scheme is illustrated in Fig. 1. The use of hydrogen caps simplifies the mapping of the partitioning problem to a graph, as there are no spurious interactions between the fragments and the cap molecules (see Sect. 2.4 below). We note that by capping the peptide bond with only hydrogen atoms, the properties of the former peptide bond will be described inaccurately. This will increase the overall errors introduced by the fragmentation, and will also introduce a stronger dependence of the total errors on

the chosen partition. Thus, while the simplified MFCC scheme cannot be recommended for production calculations, it provides a good test case for the development and assessment of new algorithms for the fragmentation of proteins.

When considering individual amino acids as smallest possible fragments, a quantum-chemical fragmentation method requires to partition the set consisting of the N amino acid residues, $V = \{1, \dots, N\}$ into disjoint, non-empty subsets V_1, \dots, V_k (corresponding to fragments) such that each amino acid is assigned to exactly one subset, i.e., $\bigcup_i V_i = V$ and $V_i \cap V_j = \emptyset$ for $i \neq j$. Here, we restrict ourselves to the problem formulation where each V_i is a connected part of the protein’s main chain. Such a choice of fragments defines a partition $\Pi = \{V_1, \dots, V_k\}$ of the protein, and the accuracy of the results obtained with a quantum-chemical fragmentation method will depend on the chosen partition Π . Here, we want to determine this partition such that a suitably defined error — or an estimate for such an error — will be minimized.

The required computational effort of the quantum-chemical calculations will depend on the number of fragments k and on the maximum size of the fragments $n_{\max} = \max_i |V_i|$. These can be connected by defining an imbalance ϵ such that

$$n_{\max} \leq (1 + \epsilon) \left\lceil \frac{N}{k} \right\rceil, \quad (2)$$

where $\lceil x \rceil$ denotes the smallest integer greater than or equal to x . For $\epsilon = 0$ the partition is balanced. Here, our goal is to find an optimal partition along the protein’s main chain for a given number of fragments k and imbalance ϵ , which implies a certain maximum size of the fragments n_{\max} . For quantum-chemical fragmentation methods, it might be advantageous to allow for some imbalance of the fragment sizes and we choose $\epsilon = 0.33$ throughout this work.

2.2 Definition of the fragmentation error

In this work, we focus on the application of fragmentation methods for the calculation of local properties, e.g., protein–ligand interaction energies, the properties of an enzymatic reaction center, or local spectroscopic properties. Thus, we are interested in the accurate description of the effect of the protein on a specific *region of interest* (RoI).

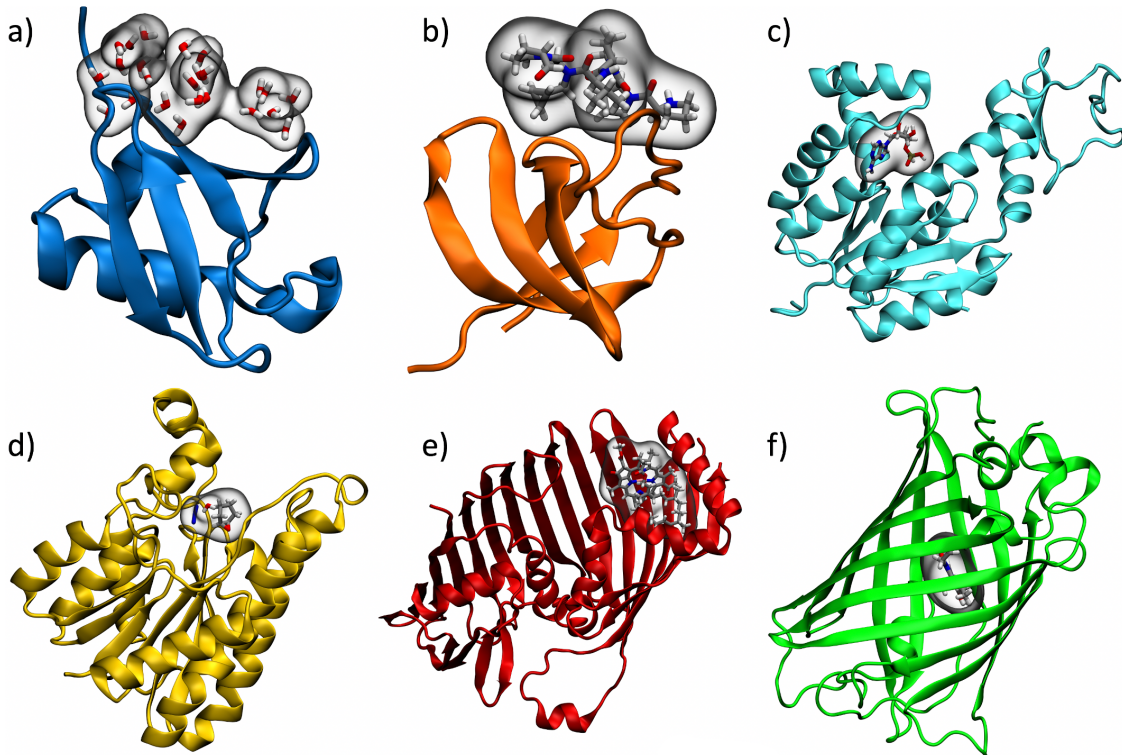


Figure 2: The test cases considered in the work for the calculation of local target properties with quantum-chemical fragmentation methods. The proteins are shown in a cartoon representation, whereas the respective binding partners, substrates, or chromophores that define our region of interest (RoI) are shown in an atomistic representation and highlighted. (a) Ubiquitin, (b) Sem5 SH3 Domain, (c) adenylate kinase, (d) halohydrin dehalogenase G (HheG), (e) Fenna-Matthews-Olson complex (FMO), and (f) green fluorescent protein (GFP).

Prototypical targets, which we will use as our test cases in the following, are shown in Fig. 2. For protein–ligand interactions, we consider the interaction of ubiquitin with ligands or other proteins³² (see Fig. 2a) and the interaction of the *Caenorhabditis elegans* adapter protein Sem5 Src homology 3 (SH3) domain with a peptoid inhibitor^{38,48} (see Fig. 2b).

As examples of enzymatic reaction centers, we consider the interaction of adenylate kinase with its substrate adenosine monophosphate³⁸ (see Fig. 2c) as well as the interaction of halohydrin dehalogenase G (HheG) with a cyclohexene oxide, an azide and a water molecule in its binding pocket⁴⁹ (see Fig. 2d). Moreover, as test cases in which local spectroscopic properties are of interest, we consider a monomer taken from the Fenna-Matthews-Olsen complex (FMO)^{50–52} (see Fig. 2e) as well as the green fluorescent protein (GFP)^{7,53,54} (see Fig. 2f). In these examples, the binding partner of the protein, the substrate of the enzyme, or the relevant chromophore define the respective RoIs, which are also highlighted in Fig. 2. More details on each of our test cases as well as the choice of the RoI will be presented in Sects. 3 and 4.

The fragmentation of the protein introduces an error in its total electron density,

$$\Delta\rho_{\text{tot}}(\mathbf{r}) = \rho_{\text{tot}}^{\text{super}}(\mathbf{r}) - \rho_{\text{tot}}^{\text{fragm}}(\mathbf{r}), \quad (3)$$

where $\rho_{\text{tot}}^{\text{super}}(\mathbf{r})$ is the electron density obtained from a supermolecular calculation for the full protein. This error in the electron density translates to an error in the electrostatic potential within the RoI,

$$\Delta V(\mathbf{r}) = \int \frac{\Delta\rho_{\text{tot}}(\mathbf{r}')}{|\mathbf{r} - \mathbf{r}'|} d^3r' = V_{\text{super}}^{\text{Coul}}(\mathbf{r}) - V_{\text{fragm}}^{\text{Coul}}(\mathbf{r}), \quad (4)$$

where $V_{\text{super}}^{\text{Coul}}(\mathbf{r}) = \int \frac{\rho_{\text{tot}}^{\text{super}}(\mathbf{r}')}{|\mathbf{r} - \mathbf{r}'|} d^3r'$ is the Coulomb potential obtained from a full, supermolecular calculation and $V_{\text{fragm}}^{\text{Coul}}(\mathbf{r}) = \int \frac{\rho_{\text{tot}}^{\text{fragm}}(\mathbf{r}')}{|\mathbf{r} - \mathbf{r}'|} d^3r'$ is the one obtained with the fragmentation method. When considering protein–ligand interaction energies, the error in the electrostatic interaction energy is given by,

$$\Delta E = \int \rho_{\text{RoI}}(\mathbf{r}) \Delta V(\mathbf{r}) d^3r, \quad (5)$$

where $\rho_{\text{RoI}}(\mathbf{r})$ is the electron density of the ligand that constitutes the RoI, i.e., the error in the electrostatic potential is weighted with the electron density defining the RoI. When em-

employing quantum-chemical fragmentation methods, this error in the electrostatic interaction energy ΔE should be kept as small as possible.

Of course, ΔE might be susceptible to error compensation between the contributions of different parts of the RoI. These will be sensitive to the specific definition of the RoI and the choice of $\rho_{\text{RoI}}(\mathbf{r})$. Therefore, we define an absolute error as

$$\Delta_{\text{abs}} = \int \rho_{\text{RoI}}(\mathbf{r}) |\Delta V(\mathbf{r})| d^3r. \quad (6)$$

This absolute error is an upper bound for the error in the electrostatic interaction energy, i.e., $\Delta E \leq \Delta_{\text{abs}}$. It can also be expected that Δ_{abs} will control the error in spectroscopic properties that are localized in the RoI. In this work, our goal is to determine the partition Π such that in a fragmentation calculation this absolute fragmentation error is minimized, subject to suitable constraints on the number of fragments and the imbalance.

2.3 Protein fragmentation as graph partitioning problem

The problem of partitioning proteins for quantum-chemical fragmentation methods can be phrased as a version of the *graph partitioning* problem considered in computer science.⁴⁵ A graph $G = (V, E)$ consists of a set of nodes (or vertices) V and a set of edges E , with each edge connecting two nodes (we exclude self-loops). A *weighted graph* is a graph with a weight function $w(E)$, assigning an *edge weight* to each edge.

A protein consists of a linear main chain of amino acids, and the fragmentation schemes considered here use groups of amino acid residues as fragments. Therefore, the most straightforward way to map a protein to a graph is by using the individual amino acids as nodes V . Fig. 3 illustrates this for the example of a β -hairpin. The eleven amino acids can be seen in an atomistic representation in Fig. 3a, whereas a graph representation in which the nodes are shown as yellow colored circles is presented in Fig. 3b.

Each edge $\{u, v\}$ in a graph connects two nodes u and v , and when representing a protein

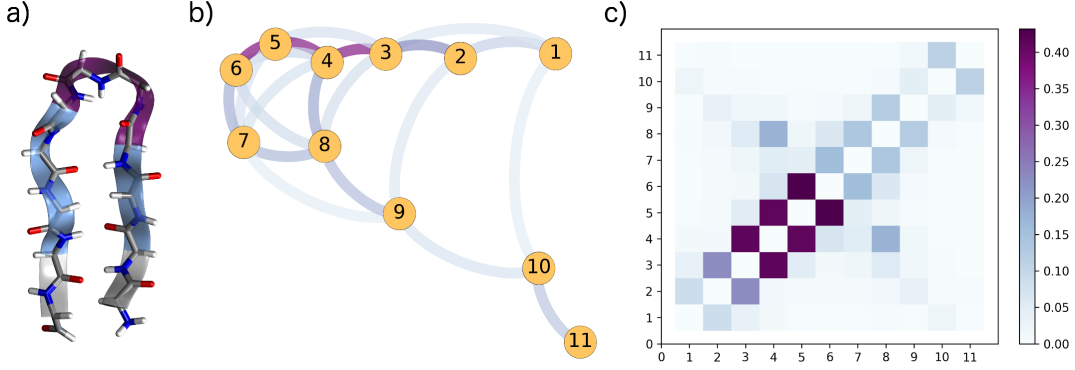


Figure 3: Illustration of the representation of proteins by a weighted graph for the example of a β -hairpin structure. (a) β -hairpin structure in atomistic and cartoon representation. (b) 2D representation of the corresponding weighted graph. The nodes are shown as yellow circles which are connected by edges. The weight of each edge is encoded in its color. (c) Matrix representation of the complete protein graph.

as a graph, the edges connect the amino acids with each other. The most obvious choice is to connect the amino acids along the backbone chain with edges $\{u, u + 1\}$, representing the bonded interactions. This leads to a linear graph representing the primary structure of the protein. However, in proteins the main chain folds into a three-dimensional structure, stabilized by the non-bonded interactions between the individual amino acids. To reflect this, additional edges $\{u, v\}$ are introduced, representing non-bonded interactions between two amino acids. All edges are assigned a suitable weight (see below). This is shown in Fig. 3b for the β -hairpin example, where the weight is encoded in the color of the edges. A graph can be represented by an $N \times N$ -matrix with the edge weights (or zero if no edge is present between two nodes) as entries (see Fig. 3c). In the simplest approach, all amino acids in a protein can be connected by edges, the resulting graph is then called *complete*.

With such a graph representation, defining a fragmentation of a protein becomes equivalent to partitioning the nodes of the graph into subsets, i.e., to a graph partition $\Pi = \{V_1, \dots, V_k\}$ (cf. Sect. 2.1), possibly subject to additional constraints. Here, we restrict ourselves to partitions in which each subset is a connected sequence of nodes along the main chain of the protein, i.e., for a graph with ascending node IDs according to the node's main chain position, each subset must contain nodes within a continuous ID range.

To determine this partition such that the expected fragmentation error is minimized, we define the weight $w(u, v)$ of the edge $\{u, v\}$ as the expected fragmentation error Δ_{abs} that arises if the two nodes (i.e., amino acids) u and v are assigned to different fragments. Thus, an estimate for the expected total fragmentation error that arises when using the partition Π is given by

$$\Delta_{\text{abs}}(\Pi, G) \approx C(\Pi, G) = \sum_{\substack{V_i, V_j \in \Pi \\ i \neq j}} \sum_{u \in V_i} \sum_{v \in V_j} w(u, v), \quad (7)$$

that is, as the sum of the weights of all edges that need to be cut when partitioning the graph. Finding the general partition $\Pi_{k, \epsilon}$ (without the restriction of a continuous ID range per block) that minimizes this *edge cut weight* $C(\Pi, G)$ for a given number of fragments k and a given imbalance ϵ is known as *graph partitioning* in computer science. The general problem is \mathcal{NP} -hard (and thus no efficient algorithm exists to solve it exactly), but fast algorithms have been developed that are able to find high-quality solutions.⁴⁵ Previously, we have investigated different available algorithms, and have adapted those to the specific constraints that arise when considering quantum-chemical fragmentation methods.⁴⁶ The restricted problem version we consider in this paper, in turn, can be solved exactly in polynomial time. Further details on the graph partitioning algorithm used here are presented below in Sect. 2.5.

2.4 Calculation of the edge weights

For a given partition $\Pi = \{V_1, \dots, V_k\}$, our simplified MFCC scheme calculates the total electron density according to Eq. (1), where $\rho_i(\mathbf{r})$ corresponds to the electron density calculated for a fragment consisting of the amino acid residues in the fragments V_i (suitably capped using hydrogen atoms as described above), whereas $\rho_j^{\text{cap}}(\mathbf{r})$ are the densities of the corresponding dihydrogen cap molecules.

To approximate the fragmentation error of a given partition, we consider a simplified

two-body expansion in terms of single amino acid fragments, i.e.,

$$\rho_i(\mathbf{r}) = \sum_{u \in V_i} \rho_u(\mathbf{r}) - \sum_j \rho_j^{\text{cap}}(\mathbf{r}) + \sum_{u,v \in V_i} \Delta\rho_{uv}^{(2)}(\mathbf{r}) \quad (8)$$

with

$$\Delta\rho_{uv}^{(2)}(\mathbf{r}) = \rho_{uv}(\mathbf{r}) - \rho_u(\mathbf{r}) - \rho_v(\mathbf{r}) - \rho_{uv}^{\text{cap}}(\mathbf{r}) \quad (9)$$

for pairs of amino acids that are directly connected by a peptide bond and with

$$\Delta\rho_{uv}^{(2)}(\mathbf{r}) = \rho_{uv}(\mathbf{r}) - \rho_u(\mathbf{r}) - \rho_v(\mathbf{r}) \quad (10)$$

for all other pairs of amino acids. Here, $\rho_{uv}(\mathbf{r})$ is the electron density of a fragment consisting of the suitably capped amino acid residues u and v , $\rho_u(\mathbf{r})$ and $\rho_v(\mathbf{r})$ are the electron densities of the suitably capped single amino acids residues u and v , respectively, and $\rho_{uv}^{\text{cap}}(\mathbf{r})$ is the cap molecule compensating for the caps introduced when cutting the peptide bonds between amino acids u and v . We note that the treatment of the cap molecules in this simplified two-body expansion is not fully consistent, as interactions between the amino acid residues and the cap molecules are neglected (see Ref. 47 for a formulation of the many-body expansion using the inclusion–exclusion principle that addresses this issue). However, for the simplified MFCC scheme using hydrogen caps considered here, we find that neglecting these interactions is justified (see Sect. 3.1).

Using the above two-body expansion in terms of single amino acids for both the super-molecular electron density $\rho_{\text{tot}}^{\text{super}}(\mathbf{r})$ and the fragment electron densities $\rho_i(\mathbf{r})$, we obtain

$$\Delta\rho_{\text{tot}}(\mathbf{r}) = \sum_{\substack{V_i, V_j \in \Pi \\ i \neq j}} \sum_{u \in V_i} \sum_{v \in V_j} \Delta\rho_{uv}^{(2)}(\mathbf{r}) \quad (11)$$

and

$$\Delta V(\mathbf{r}) = \sum_{\substack{V_i, V_j \in \Pi \\ i \neq j}} \sum_{u \in V_i} \sum_{v \in V_j} \Delta V_{uv}^{(2)}(\mathbf{r}), \quad (12)$$

with $\Delta V_{uv}^{(2)}(\mathbf{r}) = \int \frac{\rho_{uv}^{(2)}(\mathbf{r}')}{|\mathbf{r} - \mathbf{r}'|} d^3 r'$. Thus, the error in the electrostatic interaction energy [cf. Eq. (5)] can be approximated as

$$\Delta E \approx \Delta E^{(2)} = \sum_{\substack{V_i, V_j \in \Pi \\ i \neq j}} \sum_{u \in V_i} \sum_{v \in V_j} \int \rho_{\text{RoI}}(\mathbf{r}) \Delta V_{uv}^{(2)}(\mathbf{r}) d^3 r, \quad (13)$$

and the absolute fragmentation error [cf. Eq. (6)] can be approximated as

$$\Delta_{\text{abs}} \approx \Delta_{\text{abs}}^{(2)} = \int \rho_{\text{RoI}}(\mathbf{r}) \left| \sum_{\substack{V_i, V_j \in \Pi \\ i \neq j}} \sum_{u \in V_i} \sum_{v \in V_j} \Delta V_{uv}^{(2)}(\mathbf{r}) \right| d^3 r. \quad (14)$$

For this two-body approximation of the absolute fragmentation error we can establish an upper bound,

$$\Delta_{\text{abs}}^{(2)} \leq \sum_{\substack{V_i, V_j \in \Pi \\ i \neq j}} \sum_{u \in V_i} \sum_{v \in V_j} \int \rho_{\text{RoI}}(\mathbf{r}) \left| \Delta V_{uv}^{(2)}(\mathbf{r}) \right| d^3 r. \quad (15)$$

By defining the edge weights of our graph representation as

$$w(u, v) = \int \rho_{\text{RoI}}(\mathbf{r}) \left| \Delta V_{uv}^{(2)}(\mathbf{r}) \right| d^3 r, \quad (16)$$

the edge cut weight $C(\Pi, G)$ thus provides an upper bound for the two-body approximation $\Delta_{\text{abs}}^{(2)}$ of the absolute fragmentation error Δ_{abs} , which in turn provides an upper bound for the two-body approximation of the error in the electrostatic interaction energy, i.e.,

$$|\Delta E^{(2)}| \leq \Delta_{\text{abs}}^{(2)} \leq C(\Pi, G). \quad (17)$$

Note that this error bound cannot be expected to be tight. Thus, the edge cut weight

$C(\Pi, G)$, which is minimized by graph partitioning algorithms, is not equal to the fragmentation error. Nevertheless, it can be expected that by reducing this upper bound, also the fragmentation error will be reduced.

In Sect. 3, we will (a) assess the accuracy of the simplified two-body expansion for estimating the fragmentation error and (b) explore the application of graph partitioning algorithms for systematically reducing the fragmentation error in our simplified MFCC scheme.

2.5 Dynamic Programming Graph Partitioning Algorithm

Our restricted version of the graph partitioning problem, in which we search for continuous fragments along the main chain (cf. Section 2.3), leads to the following formulation: Given a graph $G = (V, E)$ with ascending node IDs according to the node's main chain position, an integer k and a maximum imbalance ϵ , find a k -partition $\Pi_{k,\epsilon}$ which respects the balance constraints, minimizes the edge cut weight $C(\Pi, G)$ and satisfies $v_j \in V_i \wedge v_j + l \in V_i \rightarrow v_j + 1 \in V_i$ for all $l \in \mathbb{N}^+, 1 \leq j < n, 1 \leq i \leq k$ (*continuous node constraint*).

Finding fragments with continuous node IDs is equivalent to finding a set of $k-1$ *delimiter nodes* $v_{d_1}, v_{d_2}, \dots, v_{d_{k-1}}$ that separate the fragments. More precisely, delimiter node v_{d_j} belongs to fragment j , $1 \leq j \leq k-1$. Consider the delimiter nodes in ascending order. Given the node v_{d_2} , the optimal placement of node v_{d_1} only depends on edges among nodes $u < v_{d_2}$, since all edges $\{u, v\}$ from nodes $u < v_{d_2}$ to nodes $v > v_{d_2}$ are cut no matter where v_{d_1} is placed. Placing node v_{d_2} thus induces an optimal placement for v_{d_1} , using only information from edges to nodes $u < v_{d_2}$. With this dependency of the positions of v_{d_1} and v_{d_2} , placing node v_{d_3} similarly induces an optimal choice for v_{d_2} and v_{d_1} , using only information from nodes smaller than v_{d_3} . The same argument can be continued inductively for nodes $v_{d_4} \dots v_{d_k}$.

This insight is used by our algorithm, which is based on the dynamic programming paradigm. It iteratively computes the optimal placement of $v_{d_{j-1}}$ for all possible values of v_{d_j} . Finding the optimal placements of $v_{d_1}, \dots, v_{d_{j-1}}$ given a delimiter v_{d_j} at node i is equivalent to the subproblem of partitioning the first i nodes into j fragments, for increasing

values of i and j . When N nodes and k fragments are reached, the desired global solution is found. For more details, we refer to our previous paper.⁴⁶

2.6 Computational Details

All quantum-chemical calculations were performed using the Amsterdam Density Functional (ADF) package^{55,56} using density-functional theory (DFT) with the BP86 exchange–correlation functional^{57,58} and a Slater-type DZP basis set.⁵⁹ The complete workflow for the construction of the graph representation as well as for our quantum-chemical fragmentation calculations using the simplified MFCC scheme has been implemented in the PyADF scripting framework.⁶⁰ PyADF Version 0.97, which can be used to reproduce all calculations presented here, is available under the GPL v3 license at Ref. 61.

In the construction of the graph representation, we included edges only between pairs of amino acids with a maximum distance of five amino acid units along the main chain or with a maximum distance of 2.5 Å through space. The edge weights were calculated according to Eq. (16) from DFT calculations for the individual amino acids as well as the corresponding pairs. The integration was performed using ADF’s integration grid for the respective RoI.

The graphs were then exported to the Chaco/METIS format⁶² to enable the use of standard graph partitioning algorithms available in a dedicated fork of the NetworkKit package⁶³ which implements the DP algorithm described above. The resulting partition was then imported into PyADF in order to perform the quantum-chemical fragmentation calculation.

Details on the protein structures used as our test cases are given in Sects. 3 and 4. All protein crystal structures were saturated with hydrogen atoms using Openbabel^{64,65} to achieve a neutral protonation state for all amino acids. 3D visualizations of the protein structures were created with VMD⁶⁶ and its build-in tools. All plots have been prepared using Python and Matplotlib^{67,68} in Jupyter notebooks. Graph equilibrations and visualizations were performed with gephi.^{69,70}

A data set containing molecular structures of all proteins and the corresponding RoIs,

the constructed graph representation, the resulting partitions, raw data for all the figures as well as PyADF input files and Jupyter notebooks used for data analysis and for producing all figures is available in the Zenodo repository at Ref. 71.

3 Initial test case: Ubiquitin

As an initial test case, we employ the small protein ubiquitin, which has been used previously as a test case for the 3-FDE scheme.^{31,32} Ubiquitin (PDB code: 1UBQ⁷²) consists of 76 amino acids, which still allows for a supermolecular DFT calculation that can be used as reference. As the crystal structure does not come with a specific binding partner, a cluster of water molecules placed in the face region of ubiquitin was used as RoI.³² To build this water cluster, the whole protein was solvated with TIP3P water, the coordinates of the solvent molecules were energy minimized for 100 steps and a short molecular dynamics simulation of 20 ps was performed with VMD and NAMD^{73,74} using a classical force field (Charmm27^{75,76}). After this procedure the 24 water molecules within a distance of 5 Å around the residues Leu8, Ile44 and Val70 were assigned to our RoI (see Fig. 2a).

3.1 Assessment of error estimation

First, we assess the different measures of the fragmentation error defined in Sect. 2.2 as well as the corresponding error estimates introduced in Sect. 2.4 for the ubiquitin test case. The most straightforward way to partition a protein into small subsystems is to use a naïve partitioning algorithm, in which the protein is partitioned into fragments containing a repeating number of amino acids along the backbone chain.^{32,38} Thus, this naïve partition is defined by the chosen number of amino acids per fragment n_{\max} . We note that in this case, the last fragment at the end of the peptide chain might be smaller. Therefore, for $n_{\max} \geq N/2$, where N is the total number of amino acids, the protein is always partitioned into two fragments and the only difference is the position of the cut along the backbone chain.

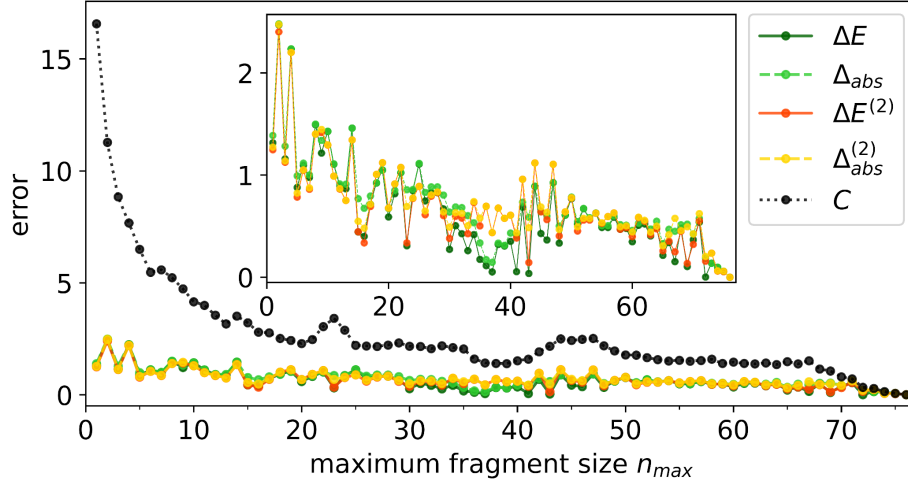


Figure 4: Comparison of fragmentation error measures ΔE (solid dark green line), Δ_{abs} (dashed green line) and error estimates $\Delta E^{(2)}$ (solid red line), $\Delta_{\text{abs}}^{(2)}$ (dashed yellow line), C (dotted black line) for the ubiquitin test case using naïve partitions with different maximum number of amino acids per fragment n_{max} . The inset shows the same data but excludes C .

In Fig. 4, the different fragmentation error measures are plotted for such a naïve partition with an increasing number n_{max} of amino acids per fragment. Here, the error in the electrostatic interaction energy ΔE [cf. Eq. (5)] (solid dark green line) and the absolute error Δ_{abs} [cf. Eq. (6)] (dashed green line) have been calculated using the difference of the electron density and Coulomb potential obtained from a full, supermolecular DFT calculation of ubiquitin and from the respective simplified MFCC calculations. The electron density ρ_{RoI} has been obtained from a DFT calculation of the 24 water molecules assigned to the RoI. Both error measures are in rather good agreement and show a similar trend. As expected, the absolute error Δ_{abs} is always larger than the error in the electrostatic interaction energy ΔE , because in the latter positive and negative deviations of the Coulomb potential from the supermolecular reference can cancel each other.

Independent of the error measure, the graphs do not show a consistent decrease of the fragmentation error as the fragment size n_{max} is increased. Instead, there are rather large fluctuations in the fragmentation error. Thus, the number of cuts between the fragments is not decisive for the accuracy of the fragmentation, but the main impact seems to be given

by the specific positions and distributions of the cuts between the fragments.

The corresponding error estimates $\Delta E^{(2)}$ [cf. Eq. (13)] and $\Delta_{\text{abs}}^{(2)}$ [cf. Eq. (14)] are included in Fig. 4 as solid red and dashed yellow line, respectively. Altogether, these are in rather good agreement with the corresponding error measures. There are, however, some partitions (e.g., for fragments sizes n_{max} between 35 and 40) where larger differences are found. Nevertheless, the overall comparison for ubiquitin confirms that the two-body approximation for the electron density, on which our error estimates are based, is sufficiently accurate and that neglecting the interaction between the hydrogen caps and the fragments is justified for our simplified MFCC scheme.

Finally, the edge cut weight $C(\Pi, G)$ [cf. Eq. (7)] calculated using the edge weights as defined in Eq. (16) is also shown Fig. 4 (dotted black line). This edge cut weight constitutes an upper bound for the absolute error estimate $\Delta_{\text{abs}}^{(2)}$. For our test case, it is always significantly larger than the corresponding error estimates, but roughly follows a similar trend, i.e., it decreases as the fragment size n_{max} is increased. Whether the edge cut weight is nevertheless useful for systematically reducing the fragmentation error will be explored in the following.

3.2 Application of graph partitioning algorithms

Graph partitioning algorithms, such as the exact dynamic programming (DP) algorithm described in Sect. 2.5, can be applied to find a partition of the graph representation of a protein that (approximately) minimizes the edge cut weight $C(\Pi, G)$. With the definition of the edge weights given by Eq. (7), this partition will thus (approximately) minimize an upper bound for our estimate $\Delta_{\text{abs}}^{(2)}$ of the absolute error Δ_{abs} .

Fig. 5a shows the edge cut weight C of the partition obtained with the DP algorithm and an imbalance of $\epsilon = 0.33$ (blue triangles) as a function of the number of subsystems k , which is used as input parameter in the DP algorithm. The maximum number of amino acids per fragment n_{max} corresponding to a given k according to Eq. (2) is included as gray bars. For comparison, the edge cut weight C obtained with the naïve partitioning scheme is also

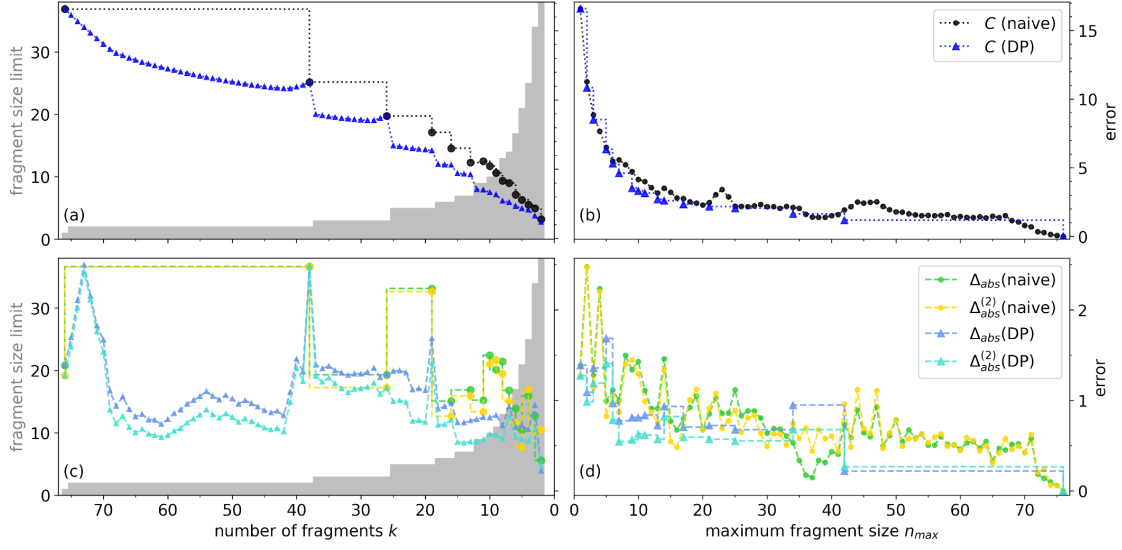


Figure 5: Comparison of the partitions obtained by the DP algorithm (triangles) and the corresponding naïve partitions (circles). (a,b) Comparison of the edge cut weight. (c,d) Comparison of the absolute error Δ_{abs} (green circles and blue triangles) and the corresponding error estimate $\Delta_{\text{abs}}^{(2)}$ (yellow circles and cyan triangles). In (a) and (c) the horizontal axis shows the number of fragments k . The corresponding fragment size limit n_{\max} applicable in the DP algorithm is shown as gray bars. In (b) and (d), the horizontal axis shows the maximum number of amino acids per fragment n_{\max} . See text for details.

included (black circles). Note that a naïve partition is not available for arbitrary numbers of fragments k , but only for $k = \lceil \frac{N}{n_{\max}} \rceil$ with $n_{\max} = 1, 2, \dots$ (black circles). For values of k between those for which a naïve partition is available, $n_{\max} = \lceil \frac{N}{k} \rceil$ is used (black dotted line), i.e., the naïve partition using a smaller number of fragments but the same maximum fragment size. Note that n_{\max} in the naïve partition and in the DP algorithm do not agree because the naïve partition implies a balanced partition ($\epsilon = 0$), whereas $\epsilon = 0.33$ is used in the DP algorithm.

Except for rather large numbers of fragments, the DP algorithm is able to find partitions with a lower C for almost all k . For $k = 76$, $k = 38$, and $k = 26$ the DP algorithm results in the corresponding naïve partition. In these cases, the choice of an imbalance of $\epsilon = 0.33$ requires that all fragments have the same size ($n_{\max} = 1, 2, 3$, respectively), which restricts the DP algorithm to the naïve partition. Thus, the partition found by the DP algorithm is always at least as good as the naïve partition, and it improves upon the latter if sufficient degrees of freedom are available. The improvement in the edge cut weight C brought about by the DP algorithm is particularly obvious for k between 5 and 20 fragments, which correspond to fragment sizes between 5 and 21 that would be feasible in large-scale applications of quantum-chemical fragmentation methods.

However, for the computational efficiency in quantum-chemical fragmentation methods, the size of the individual fragments is key, while the number of fragments is less important, in particular if the fragment calculations can be executed in parallel. Therefore, Fig. 5b shows an alternative presentation of the same data, in which n_{\max} is used as parameter on the horizontal axis. This way, the horizontal axis directly corresponds to the computational effort for the individual quantum-chemical calculations.

Here, a naïve partition is available for each integer $n_{\max} \leq N$. For the DP algorithm, different numbers of fragments k can result in the same maximum fragment size n_{\max} according to Eq. (2). Therefore, we apply the DP algorithm for all fragment numbers k that result in the same n_{\max} and choose the partition $\Pi_{n_{\max}, \epsilon}$ that minimizes the edge cut weight,

i.e.,

$$C(\Pi_{n_{\max}, \epsilon}, G) = \min_{k \rightarrow n_{\max}} C(\Pi_{k, \epsilon}, G). \quad (18)$$

It is possible that no k results in a given integer n_{\max} if the chosen maximum fragment size becomes large. In this case, the largest integer k that results in an n_{\max} that is smaller than or equal to the chosen n_{\max} is used and indicated by the blue dotted line.

For small maximum fragment size up to four amino acids per fragment, there is no or only little freedom to optimize the partition and the DP algorithm does not find better partitions than the naïve approach. Starting at a maximum fragment size of five, the DP algorithm consistently outperforms the naïve approach and is able to find a partition with a lower edge cut weight.

The edge cut weight C is only an upper bound for the error estimate $\Delta_{\text{abs}}^{(2)}$, which approximates the absolute fragmentation error Δ_{abs} . Therefore, we need to compare whether the reduction of C for the partition obtained with the DP algorithm also corresponds to a reduction of $\Delta_{\text{abs}}^{(2)}$ and Δ_{abs} . Fig. 5c and d compare these for the partition obtained from the DP algorithm (blue and cyan triangles) and the naïve partition (green and yellow circles) as a function of the number of fragments k and of the maximum number of amino acids per fragment n_{\max} , respectively.

First, we note that the error estimate $\Delta_{\text{abs}}^{(2)}$ follows same trends as Δ_{abs} . However, some differences appear, which are larger for the partitions from the DP algorithm than for the naïve partition, for instance for 40–70 fragments and for 20–25 fragments in Fig. 5c and for a maximum fragment size between 35 and 40 in Fig. 5d. Nevertheless, the two-body error estimate appears to be a good approximate to the absolute error that is sufficiently accurate for our purposes.

In Fig. 5c, the region that is most relevant for applications of quantum-chemical fragmentation methods is between 5 and 20 fragments, corresponding to maximum fragment sizes between 5 and 21 amino acids. Here, the DP algorithm reduces the absolute fragmentation error by about half compared to the naïve partition. In Fig. 5d, we find that the DP

algorithm consistently reduces the absolute fragmentation error for fragments of up to 30 amino acids. For very small fragments there is only little flexibility in the choice of partition and thus for fragments sizes 1, 3, and 4 the DP algorithm cannot improve upon the naïve partition. For fragment sizes of 15 and 16, the absolute fragmentation error of the partition found by the DP algorithm is slightly larger than for the naïve partition, but in these cases also the naïve partition gives a comparably small fragmentation error, probably because of fortunate error cancellation. For fragment sizes of 33 to 40 amino acids, the error estimate $\Delta_{\text{abs}}^{(2)}$ is comparable for the DP and naïve partition. However, in these cases the deviation of this error estimate from the actual absolute error is particularly large and thus the absolute error is significantly larger for the DP algorithm than for the naïve partition.

Despite some discrepancies, overall the DP algorithm improves significantly compared to the naïve partition. In the relevant region, it can reduce the absolute fragmentation error Δ_{abs} by up to a factor of two. Moreover, the DP algorithm leads to partitions for which the absolute fragmentation error tends to be reduced more consistently when increasing the maximum fragment size, whereas for the naïve partition the absolute fragmentation error can show rather large oscillations with the maximum fragment size.

Fig. 6 takes a closer look at the fragmentation of ubiquitin for a maximum fragment size of $n_{\text{max}} = 10$. The upper part of Fig. 6a shows the corresponding naïve partition in a cartoon representation of the protein structure, in which the colors indicate the different fragments, whereas the lower part visualizes the corresponding graphs. The largest edge weights appear between amino acids that are closest to the RoI defined by the water molecules, in particular for the β -turn formed by amino acids 4 – 12 and parts of the β -sheet (amino acids 65 – 71 as well as amino acids 41 – 49). For the naïve partition, several cuts appear in these important regions, such as between amino acids 70 and 71 as well as between amino acids 10 and 11. These cuts result in a large fragmentation error in the RoI.

Fig. 6b shows the corresponding partition from the DP algorithm, for which the fragmentation error is reduced significantly (see Fig. 5d). Here, all imperfections of the naïve

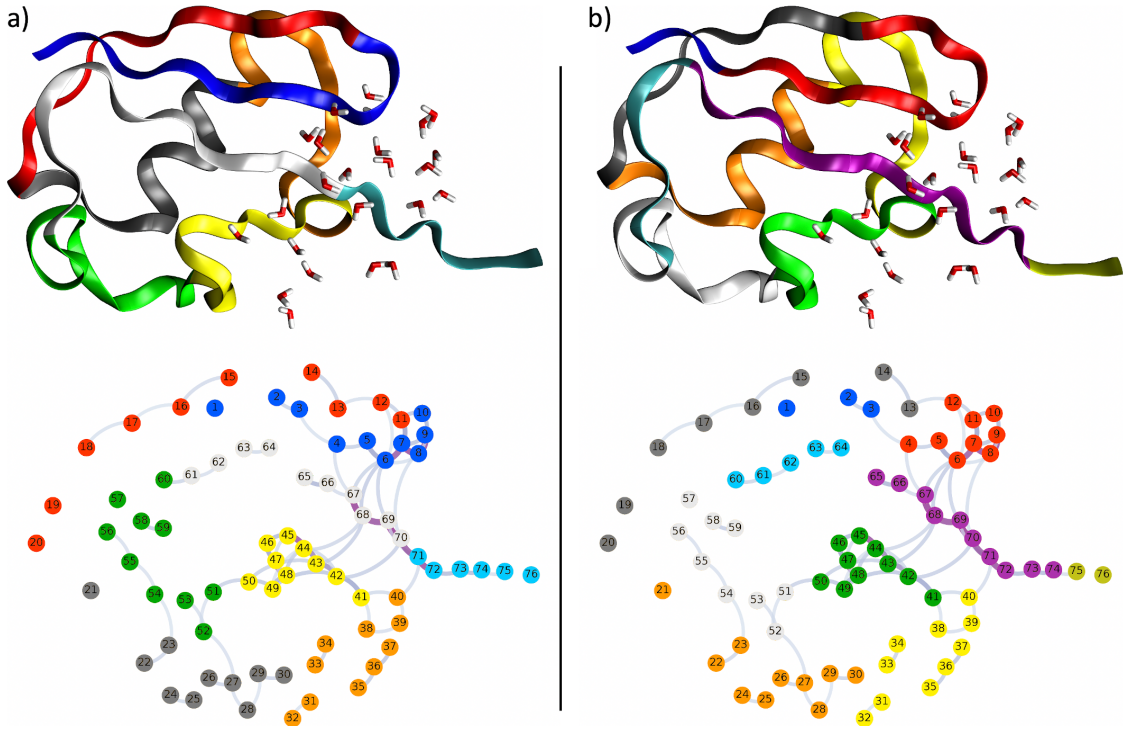


Figure 6: Visualization of (a) the naïve partition and (b) the partition found by the DP algorithm for a maximum fragment size of $n_{\max} = 10$. The upper part shows a cartoon representation of the protein in which the individual fragments are highlighted in different color. The water molecules defining the RoI are also shown. The lower part shows a representation of the corresponding graph, in which the nodes are shown as colored circles while the edge weights are represented by the thickness and color of the connecting lines (only edges with weights above a chosen threshold are shown).

partition have been obliterated and the DP algorithm optimizes the partition such that no cuts appear too close to the RoI. The β -turn (amino acids 4–12) as well as the individual strands of the β -sheet are now kept intact. Thus, by minimizing the edge cut weight, the DP algorithm automatically finds a partition in which chemically meaningful subunits of the protein are kept within the same fragment.

4 Application to Additional Test Cases

In the following, we apply the methodology established above to the further test cases shown in Fig. 2. Since for the larger proteins, a supermolecular calculation for the full protein is not easily possible, we only compare the error estimate $\Delta_{\text{abs}}^{(2)}$, which has been shown to be a sufficiently accurate approximation of the absolute fragmentation error Δ_{abs} for ubiquitin. Fig. 7 compares $\Delta_{\text{abs}}^{(2)}$ for the naïve partition and for the one obtained with the DP algorithm as function of the maximum number of amino acids per fragment n_{max} . For reference, the results for ubiquitin discussed above are shown in Fig. 7a.

As test case of protein–ligand interactions, we used the crystal structure of the Sem5 SH3 domain in a complex with a peptoid inhibitor⁴⁸ (PDB code: 3SEM,⁴⁸ see Fig. 2b). The protein consists of 58 amino acids and this example was used earlier by Antony and Grimme to assess the accuracy of protein–ligand interaction energies calculated with the MFCC scheme.³⁸ Our results for Sem5 SH3 are shown in Fig. 7b. For the naïve partition, there are large fluctuations in $\Delta_{\text{abs}}^{(2)}$ when increasing the maximum fragment size. For instance, very large errors are obtained for $n_{\text{max}} = 7$ and for $n_{\text{max}} = 17$. Except for small maximum fragment sizes ($n_{\text{max}} = 1, 4$), the DP algorithm consistently reduces $\Delta_{\text{abs}}^{(2)}$ compared to the naïve partition and $\Delta_{\text{abs}}^{(2)}$ mostly shows a monotonic decrease when increasing the maximum fragment size. The only exception is $n_{\text{max}} = 9$, for which the DP algorithm yields a slightly higher error estimate than the naïve partition.

The next two test cases are examples of enzymes, in which we consider the substrate

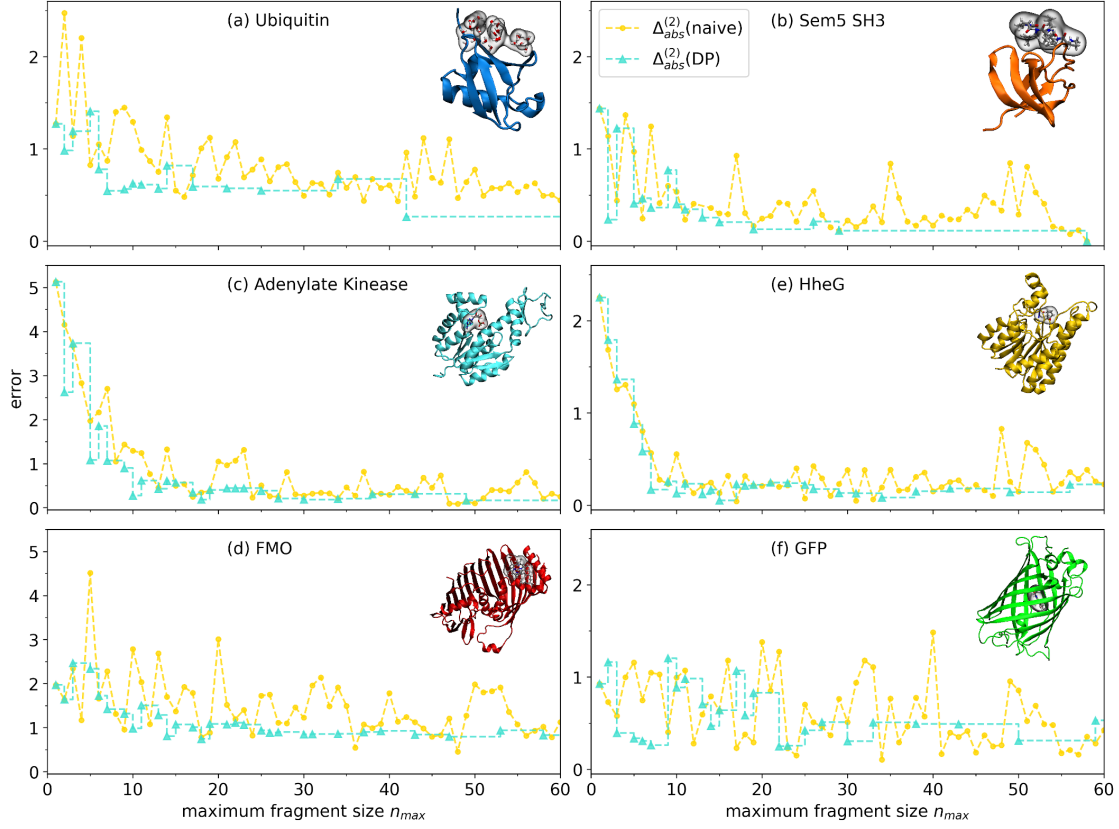


Figure 7: Comparison of the two-body estimate for the absolute fragmentation error $\Delta_{\text{abs}}^{(2)}$ for the naïve partition (yellow circles) and the partition obtained by the DP algorithm (cyan triangles) for increasing maximum number of amino acids per fragment n_{max} . (a) Ubiquitin; (b) Sem5 SH3 domain; (c) adenylate kinase; (d) Fenna-Mathews-Olson complex (FMO); (e) halohydrin dehalogenase G (HheG); (f) green fluorescent protein (GFP).

binding pocket as the RoI. First, we consider the crystal structure of adenylate kinase, which has 226 amino acids, with an adenosine monophosphate molecule in its binding pocket (PDB code: 2AK3,⁷⁷ see Fig. 2c), which is another example studied earlier by Antony and Grimme.³⁸ Second, we consider halohydrin dehalogenase G (HheG)⁴⁹ (consisting of 255 amino acids) where the RoI is represented by a cyclohexene oxide, an azide and a water molecule in its substrate binding pocket (see Fig. 2d). Here, we use a snapshot from the molecular dynamics simulations performed for this system in our earlier work.⁷⁸

The error estimates for the naïve and the DP partitions for these two systems can be found in Fig. 7c and d, showing only maximum fragment sizes up to 60 amino acids. For both systems, $\Delta_{\text{abs}}^{(2)}$ rapidly increases when increasing the maximum fragment size from 1 to ca. 10. Starting at $n_{\text{max}} = 5$, it is consistently lower for the DP algorithm than for the naïve partition. While the naïve partition shows comparably large error estimates for some specific values of n_{max} (e.g., for 20–24 for adenylate kinase and for 10, 48, and 51 for HheG), the partitions obtained by the DP algorithms do not exhibit such irregularities.

Our final two test cases are examples of photoactive proteins that contain embedded chromophores. First, we use the FMO protein (358 amino acids, see Fig. 2e), for which 3-FDE calculations of the excitation energies of the embedded bacteriochlorophylls (BChl) have been performed earlier.³⁴ Here, we used the equilibrated structure from Ref. 34 and consider the BChl 1 chromophore as the RoI. Second, we also included GFP (238 amino acids, see Fig. 2f), for which we used the available crystal structure (PDB code: 2GX2). Here, the chromophore and the resulting ends of the main amino acid chain are capped with hydrogen atoms as shown in Sect. 2.1. Note that in contrast to our four previous test cases, the RoI is fully embedded inside the protein for both FMO and GFP.

The results for GFP and FMO are presented in Fig. 7e and f. For FMO, the DP algorithm shows an overall improvement compared to the naïve partition, with only a few exceptions for values of n_{max} at which the naïve partition performs particularly well. However, for the naïve partition $\Delta_{\text{abs}}^{(2)}$ shows large fluctuations when increasing the maximum fragment size,

while a monotonic decrease is found in the DP partitions. On the other hand, for GFP the DP algorithm and the naïve approach result in partitions with overall similar error estimates, and none of the two variants clearly performs better. In GFP, the chromophore is inside the β -barrel structure at the center of the protein and most amino acids will thus be close to the RoI. Therefore, it is not easily possible to move the cuts between amino acids away from the RoI, which makes GFP a particularly difficult case for fragmentation methods, in which hardly any improvement over the naïve approach is possible.

5 Conclusions and Outlook

We have presented a methodology for systematically partitioning proteins for quantum-chemical fragmentation methods, which determines the fragmentation such that for a given maximum fragment size the expected fragmentation error in local target quantities is (approximately) minimized. To this end, we map the protein to a graph representation, in which the nodes represent amino acids and the edges are assigned weights that correspond to the fragmentation error that is expected when cutting this edge in the fragmentation. This makes it possible to apply graph partitioning algorithms provided by computer science to determine a near-optimal partition of the protein.

Here, we have chosen to minimize the error in the Coulomb potential of the protein in a specific RoI. This error, in particular the absolute fragmentation error Δ_{abs} defined here, should be closely correlated with the errors in protein–ligand interaction energies, in energy differences between different species in the active center of an enzyme, or in local spectroscopic properties of embedded chromophores. However, for specific applications in any of these areas, it might be necessary to further refine the definition of the relevant fragmentation error.

For assigning the edge weights in the graph representation of proteins, we have applied a two-body approximation, which has been shown to be sufficiently accurate for our pur-

poses. However, in the current implementation the determination of the edge weights requires quantum-chemical calculations for each pair of amino acids and thus imposes a significant computational overhead, even if interactions between distant amino acids are neglected. To address this, we plan to develop more efficient schemes in which the edge weights are parametrized in terms of simpler descriptors, such as the distances between the amino acids as well as their distance from the RoI. Similarly, more sophisticated screening strategies could significantly reduce the number of pairs for which explicit quantum-chemical calculations are required. Work in these directions is currently in progress in our research groups.

For simplicity, we only considered a simplified MFCC scheme using hydrogen caps as quantum-chemical fragmentation method in the present work. This way, interactions between the fragments and the caps can be neglected. This is generally not the case when using fragmentation methods with overlapping fragments, for which the mapping to a graph representation needs to be generalized by including additional nodes representing the caps, which will require using negative edge weights as well as additional constraints in the graph partitioning algorithms. As the present work demonstrates the usefulness of our graph-based methodology, we plan to pursue such an extension in our future work.

Using a test set of six different proteins, we could show that with the simplified MFCC scheme, our graph-based partitioning scheme using the DP algorithm consistently reduces the expected fragmentation error compared to the commonly used naïve partitioning strategy for the same maximum fragment size (i.e., for a comparable computational effort). This is particularly true for maximum fragment sizes between 5 and 20 amino acids, which are most relevant for the application of quantum-chemical fragmentation methods. In most cases, for the optimized partitions obtained with the DP algorithm, the error is systematically reduced when increasing the maximum fragment size, while large oscillations of the expected error are found for the naïve partitions. The magnitude of improvement brought about by our graph-based partitioning scheme depends on the considered proteins as well as the choice of the RoI. While for cases with a well-localized RoI, a significant reduction of the fragmentation

error is possible, we found that no or only little improvement with respect to the naïve partition for proteins in which the RoI is at the center of the protein, such as GFP.

Acknowledgments

M.W. and C.R.J. acknowledge funding from the Deutsche Forschungsgemeinschaft for the development of PyADF (Project Suresoft, JA 2329/7-1). M.v.L. and H.M. acknowledge funding from the Federal Ministry of Education and Research (Project WAVE, 01|H15004B).

References

- (1) Karplus, M. Development of Multiscale Models for Complex Chemical Systems: From H₂ to Biomolecules (Nobel Lecture). *Angew. Chem. Int. Ed.* **2014**, *53*, 9992–10005.
- (2) Hollingsworth, S. A.; Dror, R. O. Molecular Dynamics Simulation for All. *Neuron* **2018**, *99*, 1129–1143.
- (3) Chung, J. K.; Nocka, L. M.; Decker, A.; Wang, Q.; Kadlec, T. A.; Weiss, A.; Kuriyan, J.; Groves, J. T. Switch-like activation of Bruton’s tyrosine kinase by membrane-mediated dimerization. *Proc. Natl. Acad. Sci. U. S. A.* **2019**, *116*, 10798–10803.
- (4) Venable, R. M.; Krämer, A.; Pastor, R. W. Molecular Dynamics Simulations of Membrane Permeability. *Chem. Rev.* **2019**, *119*, 5954–5997.
- (5) Ryde, U.; Söderhjelm, P. Ligand-Binding Affinity Estimates Supported by Quantum-Mechanical Methods. *Chem. Rev.* **2016**, *116*, 5520–5566.
- (6) König, C.; Neugebauer, J. Quantum Chemical Description of Absorption Properties and Excited-State Processes in Photosynthetic Systems. *ChemPhysChem* **2012**, *13*, 386–425.

- (7) Bravaya, K. B.; Grigorenko, B. L.; Nemukhin, A. V.; Krylov, A. I. Quantum Chemistry Behind Bioimaging: Insights from Ab Initio Studies of Fluorescent Proteins and Their Chromophores. *Acc. Chem. Res.* **2012**, *45*, 265–275.
- (8) Curutchet, C.; Mennucci, B. Quantum Chemical Studies of Light Harvesting. *Chem. Rev.* **2017**, *117*, 294–343.
- (9) Romero-Rivera, A.; Garcia-Borràs, M.; Osuna, S. Computational tools for the evaluation of laboratory-engineered biocatalysts. *Chem. Commun.* **2016**, *53*, 284–297.
- (10) Ahmadi, S.; Herrera, L. B.; Chehelamirani, M.; Hostaš, J.; Jalife, S.; Salahub, D. R. Multiscale modeling of enzymes: QM-cluster, QM/MM, and QM/MM/MD: A tutorial review. *Int. J. Quantum Chem.* **2018**, *118*, e25558.
- (11) Ochsenfeld, C.; Kussmann, J.; Lambrecht, D. S. *Reviews in Computational Chemistry*; Wiley-VCH: New York, 2007; Vol. 23; pp 1–82.
- (12) Riplinger, C.; Sandhoefer, B.; Hansen, A.; Neese, F. Natural triple excitations in local coupled cluster calculations with pair natural orbitals. *J. Chem. Phys.* **2013**, *139*, 134101.
- (13) Roßbach, S.; Ochsenfeld, C. Influence of Coupling and Embedding Schemes on QM Size Convergence in QM/MM Approaches for the Example of a Proton Transfer in DNA. *J. Chem. Theory Comput.* **2017**, *13*, 1102–1107.
- (14) Gordon, M. S.; Fedorov, D. G.; Pruitt, S. R.; Slipchenko, L. V. Fragmentation Methods: A Route to Accurate Calculations on Large Systems. *Chem. Rev.* **2012**, *112*, 632–672.
- (15) Raghavachari, K.; Saha, A. Accurate Composite and Fragment-Based Quantum Chemical Models for Large Molecules. *Chem. Rev.* **2015**, *115*, 5643–5677.
- (16) Gordon, M. S., Ed. *Fragmentation: Toward Accurate Calculations on Complex Molecular Systems*, 1st ed.; Wiley: Hoboken, NJ, 2017.

- (17) Zhang, D. W.; Zhang, J. Z. H. Molecular fractionation with conjugate caps for full quantum mechanical calculation of protein–molecule interaction energy. *J. Chem. Phys.* **2003**, *119*, 3599–3605.
- (18) Gao, A. M.; Zhang, D. W.; Zhang, J. Z. H.; Zhang, Y. An efficient linear scaling method for ab initio calculation of electron density of proteins. *Chem. Phys. Lett.* **2004**, *394*, 293–297.
- (19) He, X.; Zhu, T.; Wang, X.; Liu, J.; Zhang, J. Z. H. Fragment Quantum Mechanical Calculation of Proteins and Its Applications. *Acc. Chem. Res.* **2014**, *47*, 2748–2757.
- (20) Gomes, A. S. P.; Jacob, Ch. R. Quantum-chemical embedding methods for treating local electronic excitations in complex chemical systems. *Annu. Rep. Prog. Chem., Sect. C* **2012**, *108*, 222.
- (21) Goez, A.; Neugebauer, J. In *Frontiers of Quantum Chemistry*; Wójcik, M. J., Nakatsuji, H., Kirtman, B., Ozaki, Y., Eds.; Springer: Singapore, 2018; pp 139–179, DOI: 10.1007/978-981-10-5651-2_7.
- (22) Wang, X.; Liu, J.; Zhang, J. Z. H.; He, X. Electrostatically Embedded Generalized Molecular Fractionation with Conjugate Caps Method for Full Quantum Mechanical Calculation of Protein Energy. *J. Phys. Chem. A* **2013**,
- (23) Jiang, N.; Ma, J.; Jiang, Y. Electrostatic field-adapted molecular fractionation with conjugated caps for energy calculations of charged biomolecules. *J. Chem. Phys.* **2006**, *124*, 114112.
- (24) Kitaura, K.; Ikeo, E.; Asada, T.; Nakano, T.; Uebayasi, M. Fragment molecular orbital method: an approximate computational method for large molecules. *Chem. Phys. Lett.* **1999**, *313*, 701 – 706.

- (25) Nakano, T.; Kaminuma, T.; Sato, T.; Akiyama, Y.; Uebayasi, M.; Kitaura, K. Fragment molecular orbital method: application to polypeptides. *Chem. Phys. Lett.* **2000**, *318*, 614–618.
- (26) Fedorov, D. G.; Kitaura, K. Extending the Power of Quantum Chemistry to Large Systems with the Fragment Molecular Orbital Method. *J. Phys. Chem. A* **2007**, *111*, 6904–6914.
- (27) Tanaka, S.; Mochizuki, Y.; Komeiji, Y.; Okiyama, Y.; Fukuzawa, K. Electron-correlated fragment-molecular-orbital calculations for biomolecular and nano systems. *Phys. Chem. Chem. Phys.* **2014**,
- (28) Fedorov, D. G. The fragment molecular orbital method: theoretical development, implementation in GAMESS, and applications. *WIREs Comput. Mol. Sci.* **2017**, *7*, e1322.
- (29) Jacob, Ch. R.; Neugebauer, J. Subsystem density-functional theory. *WIREs Comput. Mol. Sci.* **2014**, *4*, 325–362.
- (30) Wesolowski, T. A.; Shedge, S.; Zhou, X. Frozen-Density Embedding Strategy for Multilevel Simulations of Electronic Structure. *Chem. Rev.* **2015**, *115*, 5891–5928.
- (31) Jacob, Ch. R.; Visscher, L. A subsystem density-functional theory approach for the quantum chemical treatment of proteins. *J. Chem. Phys.* **2008**, *128*, 155102.
- (32) Kiewisch, K.; Jacob, Ch. R.; Visscher, L. Quantum-Chemical Electron Densities of Proteins and of Selected Protein Sites from Subsystem Density Functional Theory. *J. Chem. Theory Comput.* **2013**, *9*, 2425–2440.
- (33) Asada, N.; Fedorov, D. G.; Kitaura, K.; Nakanishi, I.; Merz, K. M. An Efficient Method to Evaluate Intermolecular Interaction Energies in Large Systems Using Overlapping Multicenter ONIOM and the Fragment Molecular Orbital Method. *J. Phys. Chem. Lett.* **2012**, *3*, 2604–2610.

- (34) Goez, A.; Jacob, Ch. R.; Neugebauer, J. Modeling environment effects on pigment site energies: Frozen density embedding with fully quantum-chemical protein densities. *Comput. Theor. Chem.* **2014**, *1040–1041*, 347–359.
- (35) Goez, A.; Neugebauer, J. Including protein density relaxation effects in first-principles embedding calculations of cofactor excitation energies. *Mol. Phys.* **2017**, *115*, 526–537.
- (36) Senn, H. M.; Thiel, W. QM/MM Methods for Biomolecular Systems. *Angew. Chem. Int. Ed.* **2009**, *48*, 1198–1229.
- (37) Morzan, U. N.; Alonso de Armiño, D. J.; Foglia, N. O.; Ramírez, F.; González Lebrero, M. C.; Scherlis, D. A.; Estrin, D. A. Spectroscopy in Complex Environments from QM–MM Simulations. *Chem. Rev.* **2018**, *118*, 4071–4113.
- (38) Antony, J.; Grimme, S. Fully ab initio protein-ligand interaction energies with dispersion corrected density functional theory. *J. Comput. Chem.* **2012**, *33*, 1730–1739.
- (39) He, X.; Zhang, J. Z. H. The generalized molecular fractionation with conjugate caps/molecular mechanics method for direct calculation of protein energy. *J. Chem. Phys.* **2006**, *124*, 184703.
- (40) Li, W.; Li, S.; Jiang, Y. Generalized Energy-Based Fragmentation Approach for Computing the Ground-State Energies and Properties of Large Molecules. *J. Phys. Chem. A* **2007**, *111*, 2193–2199.
- (41) Li, S.; Li, W.; Ma, J. Generalized Energy-Based Fragmentation Approach and Its Applications to Macromolecules and Molecular Aggregates. *Acc. Chem. Res.* **2014**, *47*, 2712–2720.
- (42) Gadre, S. R.; Shirsat, R. N.; Limaye, A. C. Molecular Tailoring Approach for Simulation of Electrostatic Properties. *J. Phys. Chem.* **1994**, *98*, 9165–9169.

- (43) Babu, K.; Gadre, S. R. Ab initio quality one-electron properties of large molecules: Development and testing of molecular tailoring approach. *J. Comput. Chem.* **2003**, *24*, 484–495.
- (44) Sahu, N.; Gadre, S. R. Molecular Tailoring Approach: A Route for ab Initio Treatment of Large Clusters. *Acc. Chem. Res.* **2014**, *47*, 2739–2747.
- (45) Buluç, A.; Meyerhenke, H.; Safro, I.; Sanders, P.; Schulz, C. In *Algorithm Engineering: Selected Results and Surveys*; Kliemann, L., Sanders, P., Eds.; Lecture Notes in Computer Science; Springer International Publishing: Cham, 2016; pp 117–158, DOI: 10.1007/978-3-319-49487-6_4.
- (46) von Looz, M.; Wolter, M.; Jacob, Ch. R.; Meyerhenke, H. In *Experimental Algorithms*; Goldberg, A. V., Kulikov, A. S., Eds.; Lecture Notes in Computer Science; Springer International Publishing, 2016; pp 353–368, DOI: 10.1007/978-3-319-38851-9_24.
- (47) Richard, R. M.; Herbert, J. M. A generalized many-body expansion and a unified view of fragment-based methods in electronic structure theory. *J. Chem. Phys.* **2012**, *137*, 064113.
- (48) Nguyen, J. T.; Turck, C. W.; Cohen, F. E.; Zuckermann, R. N.; Lim, W. A. Exploiting the Basis of Proline Recognition by SH3 and WW Domains: Design of N-Substituted Inhibitors. *Science* **1998**, *282*, 2088–2092.
- (49) Koopmeiners, J.; Diederich, C.; Solarczek, J.; Voß, H.; Mayer, J.; Blankenfeldt, W.; Schallmey, A. HheG, a Halohydrin Dehalogenase with Activity on Cyclic Epoxides. *ACS Catalysis* **2017**, *7*, 6877–6886.
- (50) Fenna, R. E.; Matthews, B. W. Chlorophyll arrangement in a bacteriochlorophyll protein from *Chlorobium limicola*. *Nature* **1975**, *258*, 573–577.

- (51) Matthews, B. W.; Fenna, R. E.; Bolognesi, M. C.; Schmid, M. F.; Olson, J. M. Structure of a bacteriochlorophyll a-protein from the green photosynthetic bacterium *Prosthecochloris aestuarii*. *J. Mol. Biol.* **1979**, *131*, 259–285.
- (52) König, C.; Neugebauer, J. Protein Effects on the Optical Spectrum of the Fenna–Matthews–Olson Complex from Fully Quantum Chemical Calculations. *J. Chem. Theory Comput.* **2013**, *9*, 1808–1820.
- (53) Zimmer, M. Green Fluorescent Protein (GFP): Applications, Structure, and Related Photophysical Behavior. *Chem. Rev.* **2002**, *102*, 759–782.
- (54) Daday, C.; Curutchet, C.; Sinicropi, A.; Mennucci, B.; Filippi, C. Chromophore–Protein Coupling beyond Nonpolarizable Models: Understanding Absorption in Green Fluorescent Protein. *J. Chem. Theory Comput.* **2015**, *11*, 4825–4839.
- (55) te Velde, G.; Bickelhaupt, F. M.; Baerends, E. J.; Fonseca Guerra, C.; van Gisbergen, S. J. A.; Snijders, J. G.; Ziegler, T. Chemistry with ADF. *J. Comput. Chem.* **2001**, *22*, 931–967.
- (56) Software for Chemistry and Materials, Amsterdam, ADF, Amsterdam density functional program. 2019; URL: <http://www.scm.com> .
- (57) Becke, A. D. Density-functional exchange-energy approximation with correct asymptotic behavior. *Phys. Rev. A* **1988**, *38*, 3098–3100.
- (58) Perdew, J. P. Density-functional approximation for the correlation energy of the inhomogeneous electron gas. *Phys. Rev. B* **1986**, *33*, 8822–8824.
- (59) Van Lenthe, E.; Baerends, E. J. Optimized Slater-type basis sets for the elements 1–118. *J. Comput. Chem.* **2003**, *24*, 1142–1156.
- (60) Jacob, Ch. R.; Beyhan, S. M.; Bulo, R. E.; Gomes, A. S. P.; Götz, A. W.; Kiewisch, K.;

- Sikkema, J.; Visscher, L. PyADF — A scripting framework for multiscale quantum chemistry. *J. Comput. Chem.* **2011**, *32*, 2328–2338.
- (61) Jacob, Ch. R.; Beyhan, S. M.; Buló, R. E.; Gomes, A. S. P.; Goetz, A. W.; Handzlik, M.; Kiewisch, K.; Klammler, M.; Ridder, L.; Sikkema, J.; Visscher, L.; Wolter, M. PYADF Version 0.97. 2020; DOI: 10.5281/zenodo.4066822, URL: <https://github.com/chjacob-tubs/pyadf-releases/tree/v0.97>.
- (62) Karypis, G. METIS. A Software Package for Partitioning Unstructured Graphs, Partitioning Meshes, and Computing Fill-Reducing Orderings of Sparse Matrices. 2013; Manual of version 5.1.0., URL: <http://glaros.dtc.umn.edu/gkhome/fetch/sw/metis/manual.pdf>.
- (63) Staudt, C. L.; Sazonovs, A.; Meyerhenke, H. NetworKit: A tool suite for large-scale complex network analysis. *Netw. Sci.* **2016**, *4*, 508–530.
- (64) O’Boyle, N. M.; Banck, M.; James, C. A.; Morley, C.; Vandermeersch, T.; Hutchison, G. R. Open Babel: An open chemical toolbox. *J. Cheminformatics* **2011**, *3*, 33.
- (65) The Open Babel package, Version 2.4.1. URL: <http://openbabel.org>.
- (66) Humphrey, W.; Dalke, A.; Schulten, K. VMD — Visual Molecular Dynamics. *J. Mol. Graphics* **1996**, *14*, 33–38.
- (67) Hunter, J. D. Matplotlib: A 2D Graphics Environment. *Comput. Sci. Eng.* **2007**, *9*, 90–95, Conference Name: Computing in Science Engineering, DOI: 10.1109/MCSE.2007.55.
- (68) MATPLOTLIB Version 3.2.1. 2020; DOI: 10.5281/zenodo.3714460, URL: <https://matplotlib.org>.
- (69) Bastian, M.; Heymann, S.; Jacomy, M. Gephi: An Open Source Software for Exploring

- and Manipulating Networks. International AAAI Conference on Weblogs and Social Media. 2009.
- (70) Gephi, Version 0.9.2. URL: <http://gephi.org> .
- (71) Wolter, M.; von Looz, M.; Meyerhenke, H.; Jacob, Ch. R. Data Set: Systematic partitioning of proteins for quantum-chemical fragmentation methods using graph algorithms. 2020; DOI: 10.5281/zenodo.4066960.
- (72) Vijay-Kumar, S.; Bugg, C. E.; Cook, W. J. Structure of ubiquitin refined at 1.8 Å resolution. *J. Mol. Biol.* **1987**, *194*, 531–544.
- (73) Kalé, L.; Skeel, R.; Bhandarkar, M.; Brunner, R.; Gursoy, A.; Krawetz, N.; Phillips, J.; Shinozaki, A.; Varadarajan, K.; Schulten, K. NAMD2: Greater Scalability for Parallel Molecular Dynamics. *J. Comput. Phys.* **1999**, *151*, 283–312.
- (74) Phillips, J. C.; Hardy, D. J.; Maia, J. D. C.; Stone, J. E.; Ribeiro, J. a. V.; Bernardi, R. C.; Buch, R.; Fiorin, G.; Hénin, J.; Jiang, W.; McGreevy, R.; Melo, M. C. R.; Radak, B. K.; Skeel, R. D.; Singharoy, A.; Wang, Y.; Roux, B.; Aksimentiev, A.; Luthey-Schulten, Z.; Kalé, L. V.; Schulten, K.; Chipot, C.; Tajkhorshid, E. Scalable molecular dynamics on CPU and GPU architectures with NAMD. *J. Chem. Phys.* **2020**, *153*, 044130.
- (75) MacKerell Jr., A. D.; Bashford, D.; Bellott, M.; Dunbrack, R. L.; Evanseck, J. D.; Field, M. J.; Fischer, S.; Gao, J.; Guo, H.; Ha, S.; Joseph-McCarthy, D.; Kuchnir, L.; Kuczera, K.; Lau, F. T. K.; Mattos, C.; Michnick, S.; Ngo, T.; Nguyen, D. T.; Prodhom, B.; Reiher, W. E.; Roux, B.; Schlenkrich, M.; Smith, J. C.; Stote, R.; Straub, J.; Watanabe, M.; Wiórkiewicz-Kuczera, J.; Yin, D.; Karplus, M. All-Atom Empirical Potential for Molecular Modeling and Dynamics Studies of Proteins. *J. Phys. Chem. B* **1998**, *102*, 3586–3616.

- (76) Mackerell, A. D.; Feig, M.; Brooks, C. L. Extending the treatment of backbone energetics in protein force fields: Limitations of gas-phase quantum mechanics in reproducing protein conformational distributions in molecular dynamics simulations. *J. Comput. Chem.* **2004**, *25*, 1400–1415.
- (77) Diederichs, K.; Schulz, G. E. The refined structure of the complex between adenylate kinase from beef heart mitochondrial matrix and its substrate AMP at 1.85 Å resolution. *J. Mol. Biol.* **1991**, *217*, 541–549.
- (78) Solarczek, J.; Klünemann, T.; Brandt, F.; Schrepfer, P.; Wolter, M.; Jacob, Ch. R.; Blankenfeldt, W.; Schallmey, A. Position 123 of halohydrin dehalogenase HheG plays an important role in stability, activity, and enantioselectivity. *Sci. Rep.* **2019**, *9*, 5106.